A subgrain-size piezometer calibrated for EBSD

R.M. Goddard[1], L. N. Hansen[1,2], D. Wallis[3,4], M. Stipp[5], C.W. Holyoke, III[6], K.M. Kumamoto[1], & D.L. Kohlstedt[2]

[1]University of Oxford, Department of Earth Sciences, South Parks Road, Oxford, OX1 3AN, UK

[2]University of Minnesota, Department of Earth and Environmental Sciences, University of Minnesota – Twin Cities, Minneapolis, Minnesota, USA

[3]Department of Earth Sciences, Utrecht University, Utrecht, 3584 CB, The Netherlands.

[4]University of Cambridge, Department of Earth Sciences, University of Cambridge, Cambridge, CB2 3EQ, U.K

[5]University of Halle, Department of Geosciences and Geography, Von-Seckendorff-Platz 3, 06120 Halle (Saale), Germany

[6]University of Akron, Department of Geosciences, 302 Buchtel Common, Akron, OH 44325-4101 USA

Corresponding author:

Rellie Goddard (rellie.goddard@gmail.com)

Key Points

1. We present a new subgrain-size piezometer calibrated for EBSD, with a 1° critical misorientation angle.
2. This subgrain-size piezometer can be applied to multiple minerals and appears to be independent of the deformation geometry.
3. This subgrain-size piezometer should be unaffected by the presence of secondary minerals and thus applicable to polymineralic rocks.

Abstract

We calibrate a subgrain-size piezometer using electron backscatter diffraction (EBSD) data collected from experimentally deformed samples of olivine and quartz. Systematic analyses of angular and spatial resolution test the suitability of each dataset for inclusion in calibration of the subgrain-size piezometer. To identify subgrain boundaries, we consider a range of critical misorientation angles and conclude that a 1° threshold provides the optimal piezometric calibration. The mean line-intercept length, equivalent to the subgrain-size, is found to be inversely proportional to the von Mises equivalent stress for datasets both with and without the Holyoke and Kronenberg (2010) correction. These new piezometers provide stress estimates from EBSD analyses of polymineralic rocks without the need to discriminate between relict and recrystallised grains and therefore greatly increase the range of rocks that may be used to constrain geodynamic models.

Plain Language Summary

Understanding the tectonic stress in the lithospheric plates is key to evaluating a breadth of geological phenomena, such as the evolution of major ductile shear zones. One method of estimating past stress magnitudes is to measure microstructural features that vary systematically with the applied stress, a technique known as ‘piezometry’. Several piezometers have been calibrated based on the size of recrystallised grains in a rock, but they are limited to domains consisting of only a single mineral, as the presence of multiple minerals inhibits grain growth. Subgrains, however, are features inside individual grains and are unaffected by the presence of other minerals. We use electron backscatter diffraction (EBSD), a scanning electron microscopy technique, to quantify the relationship between subgrain size and stress in rocks that have been deformed in a laboratory under controlled conditions, providing the first subgrain-size piezometer calibrated for EBSD. In addition, unlike many piezometers that are calibrated for a single mineral, our piezometer can be applied to each mineral in a rock. This piezometer

offers the potential to investigate the macroscopic stress and microscopic stress distributions in a wide range of rock types.

1. Introduction

Quantitative constraints on the stresses associated with past deformation events in the ductile portion of the lithosphere are key to developing and testing geodynamic models. One method of estimating past stress magnitudes is to measure microstructural elements that can be related to stress through experimental calibrations, a technique known as piezometry. Paleopiezometry has provided key estimates of the strength of continental (e.g., Kohlstedt & Weathers, 1980; Stipp et al., 2002; Weathers et al., 1979) and oceanic (e.g., Hansen et al., 2013; Jaroslow et al., 1996; Speckbacher et al. 2011; Warren & Hirth, 2006) fault zones, yielded insight into the mechanisms of localisation in outcrop-scale shear zones (e.g., Austin et al., 2008; Gueydan et al., 2005; Haertel & Herwegh, 2014; Linckens et al., 2011; Skemer et al., 2010; Skemer et al., 2013), and enabled tests of the extrapolation of laboratory-derived rheological laws to geological conditions (e.g., Behr & Platt, 2011; Hansen & Warren, 2015; Hirth et al., 2001; Stipp et al., 2002; Wex et al., 2019). Thus, paleopiezometry is an essential tool for field-based quantitative investigations of the mechanical behaviour of the lithosphere.

The most frequently used piezometers are based on the size of dynamically recrystallized grains, herein referred to as grain size (Karato et al., 1980; Rutter, 1995; Schmid et al., 1980; Stipp & Tullis, 2003; Twiss, 1986; Van der Wal et al., 1993). However, piezometers based on grain size are only applicable to rocks consisting of a single mineral. Secondary minerals may modify grain size by limiting grain-boundary mobility and thus inhibiting grain growth, an effect known as ‘pinning’ (Evans et al., 2001; Hiraga et al., 2010; Smith, 1948; Tasaka et al., 2017). As most natural rocks contain more than one mineral, pinning severely limits the applicability of grain-size piezometers.

Like grain size, subgrain size varies systematically with differential stress during steady-state deformation (Luton & Sellars, 1969; Twiss, 1986). Piezometers based on these intragranular structures

are preferable to those based on grain size for two reasons: 1) subgrain sizes are not modified by grain-boundary pinning (Hansen & Warren, 2015; White, 1979), and 2) as subgrains form over relatively small strain intervals (≤ 10%, Biberger & Blum, 1992; Ross et al., 1980) in both relict and recrystallised grains. Therefore, subgrain-size piezometry can be applied to samples subject to small strains and obviates the need to identify grains that formed by dynamic recrystallisation. Subgrain-size piezometry therefore provides a tool to evaluate past stress experienced by broader range of rocks, including polymineralic rocks (e.g., Hansen & Warren, 2015).

Relationships between applied stress and subgrain size measured using optical microscopy or transmission electron microscopy (TEM) have been established for quartz (Mercier et al., 1977), olivine (Durham & Goetze, 1977; Goetze, 1975; Karato et al., 1980; Toriumi, 1979), and calcite (Friedman & Higgs, 1981; Platt & De Bresser, 2017). In addition, subgrain-size piezometers applicable to multiple minerals have previously been proposed (Shimizu, 1998; Twiss, 1986). However, different methods for measuring microstructural features have different detection limits, which can lead to systematic offsets between piezometric relationships for the same mineral (Cross et al., 2017; Hansen et al., 2011). Currently, no subgrain-size piezometers have been calibrated for data collected by electron backscatter diffraction (EBSD), despite the relatively simple sample preparation, rapid data acquisition, and precision in misorientation angles of ± 0.5° (Humphreys, 2004) associated with this technique.

Here, we present EBSD measurements of subgrain size in experimentally deformed olivine and quartz samples and derive a single piezometric relationship for both minerals. We explore the sensitivity of the piezometric calibration to the lower cut-off of subgrain-boundary misorientation angles and provide tests for the number of intercept lines, the number of grains, and the step size required to accurately capture the subgrain size. The resulting piezometer greatly extends the range of rocks for which EBSD data can provide quantitative stress estimates.

2. Method

2.1 Sample Description

Samples from three sets of experiments conducted on quartz and olivine were analysed. The experimental conditions associated with each sample can be found in the supplementary material (Table S1). Each stress reported in Table S1 is the von Mises equivalent stress (hereafter referred to solely as the equivalent stress, σ) experienced by the sample, which is assumed to be associated with the microstructures observed at the end of the experiment. All samples were deformed in a regime in which deformation is rate-limited by the motion of dislocations.

2.1.1 Quartz Experiments

Quartz samples prepared from Black Hills Quartzite were deformed in two sets of experiments, denoted Qz-1 and Qz-2. Qz-1 samples were deformed in a Griggs apparatus at Brown University, Rhode Island (Stipp & Tullis, 2003). Qz-2 consists of samples deformed in a Griggs apparatus either at Texas A&M University or at Brown University (Holyoke & Kronenberg, 2013; Holyoke & Tullis, 2006). Both sets of experiments were conducted at a confining pressure of 1.50–1.56 GPa and temperatures in the range 800°–1100°C. Samples included in the calibration lay within recrystallisation regimes 2 and 3 as defined by Hirth and Tullis (1992), as the relationship between subgrain size and stress appears to change in regime 1 (cf., Stipp & Tullis, 2003).

The Qz-1 samples consisted of cylinders deformed in axial compression at constant displacement rates of 1.8×10^{-6}–1.7×10^{-3} mm/s. Flow stress, taken as an average of the value between 10% strain and the value at the final strain (17–41%) in each experiment, ranged between 34 ± 16 and 268 ± 40 MPa (Stipp et al., 2003).

For the Qz-2 samples, experienced either general shear or axial compression at constant equivalent strain rates of 1.6×10^{-6}–1.15×10^{-5}. Final shear strains ranged from 50% to 610%. The only

experiment deformed in axial compression in Qz-2, TMQ-7, reached a final axial strain of 15.6%. All Qz-2 samples, excluding W-1105, were deformed to their yield point. The ability of subgrains to keep pace with the stress after very little strain means the lack of steady-state conditions should not influence the piezometric calibration. Therefore the final flow stress, converted into the equivalent stress, was taken as the stress associated with the final microstructures.

Correction of the mechanical data in Qz-1 and Qz-2 for the friction on the σ_1 piston, were performed according to the procedures of Gleason and Tullis (1995) / Stipp and Tullis (2003) and Holyoke and Tullis (2006), respectively. We then compare two sets of stresses to subgrain size, either with or without a second friction correction described by Holyoke and Kronenberg (2010, 2013) to account for increased friction due to a Poisson effect on the load column during loading of the sample.

2.1.2 Olivine Experiments

Data from olivine samples deformed in a number of different axial compression and torsion experiments were compiled to form the 'Ol' dataset (Hansen et al., 2011, 2012; Pommier et al., 2015; Tasaka et al., 2016, 2017) . Polycrystalline Fo_{90} and Fo_{50} samples were fabricated from San Carlos olivine (Hansen et al., 2011) or from a combination of oxide powers and San Carlos olivine (Tasaka et al., 2017), respectively. Experiments were conducted in a servo-controlled, internally heated, gas-medium apparatus (Paterson, 1990) at the University of Minnesota, at a confining pressure of 300 MPa and temperatures of 1150°–1250°C. Equivalent strain rates were 9×10^{-6}–1.48×10^{-3} s^{-1}. Stress was measured with an internal load cell and controlled to ±1 MPa for axial compression experiments (Hansen et al., 2011) and ±2 MPa for torsion experiments (Tasaka et al., 2016). Stresses measured during torsion experiments were converted to equivalent stress following Paterson and Olgaard (2000). In axial compression experiments, maximum axial strains reached up to 20%. In torsion experiments, except PT-0966, the strain was recorded as the outer radius shear strain and reached up to 880%. For sample PT-0966 the shear strain, recorded as 500%, was calculated from an originally vertical crease in the jacket formed during the initial pressurisation of the sample.

2.2 Acquisition of Microstructural Data

For EBSD analyses, samples deformed in axial compression were cut parallel to the cylindrical axis (Hansen et al., 2011; Holyoke & Kronenberg, 2013; Stipp & Tullis, 2003). For samples deformed in torsion, tangential sections were chosen for analysis (Hansen et al., 2012; Tasaka et al., 2016, 2017). In the direct shear geometry, sections parallel to the shear direction and perpendicular to the shear plane were chosen (Holyoke & Tullis, 2006). The sectioned surfaces were prepared by polishing with diamond lapping films or suspensions with decreasing grit sizes from 30 to 0.05 μm and were generally finished by polishing with 0.03 or 0.04 μm colloidal silica.

EBSD data were collected with an FEI Quanta 650 FEG E-SEM in the Department of Earth Sciences, University of Oxford, equipped with Oxford Instruments AZtec (Version 3.3) acquisition software and a NordlysNano EBSD camera. Samples, were tilted at 70° and mapped in low vacuum (50–60 Pa, H_2O) at accelerating voltages of 20–30 kV with step sizes of 0.1–1.0 μm. Noise reduction was performed using Oxford Instruments Channel5 software. Non-indexed points with ≥ 6 indexed neighbours within the same grain were assigned the average orientation of their neighbours. In addition, pixels in images of quartz that were systematically misindexed due to pseudosymmetry were corrected by applying a rotation of 60° around [0001] (Trimby et al., 2002).

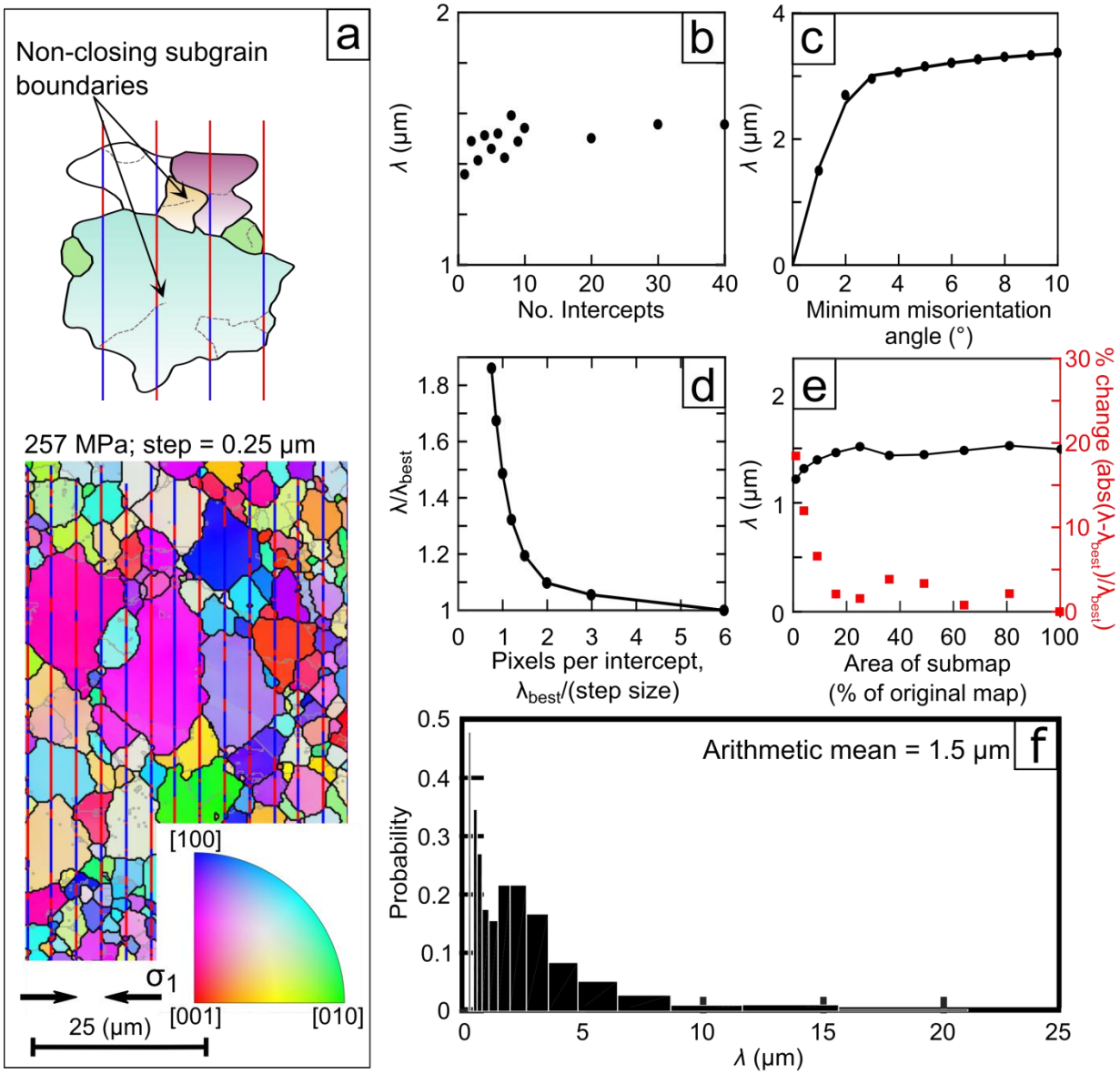

157

158

159 Figure 1: Full analysis of PI-1523 (olivine), where λ is the measured mean line-intercept length and λ_{best} is

160 the value of λ associated with the smallest step size and largest map area. (a) Schematic of the line-intercept

161 method on a map of the sample coloured by normal to the section. (b) Mean line-intercept length versus the

162 number of intercept lines taken in both the vertical and the horizontal direction. (c) Mean line-intercept length

163 versus minimum misorientation angle used to define a subgrain boundary. (d) Step-size analysis, see main text for

description. (e) Area analysis, see main text for description. (f) Histogram of mean line-intercept lengths with a logarithmic bin width.

For our piezometer, subgrains were measured using the line-intercept method. This method, compares adjacent pixels on evenly spaced lines transecting the sample (Figure 1a). Along each line, misorientations greater than a specified angle, the critical misorientation angle, are detected and the intercept length between misorientations recorded. The number of intercept lines is increased and the mean line-intercept length measured until the latter stabilises (±2.5%), thus ensuring the number of intercepts is sufficient to accurately estimate the mean value.

The line-intercept method is preferred over other grain-size measurement techniques because it includes non-closing subgrain boundaries. When analysing subgrain boundaries with small misorientation angles, it is important to include such primitive structures because subgrain boundaries do not always fully enclose an isolated region (e.g., Figure1a & Figure 2). Additional benefits compared to alternative area-based subgrain-size measurement include lower sensitivity to changes in step size (Mingard et al., 2007; Valcke et al., 2006), faster processing times (Humphreys, 2001), and lower sensitivity to anomalous clusters of data points missed during post-processing (Hansen et al., 2011).

To obtain sample averages, we use the arithmetic mean of the line-intercept lengths. This approach provides the mean spacing between all boundaries with misorientations above the chosen critical value. An alternative average, the geometric mean, is more sensitive to misindexed pixels and variations in step-size (Mingard et al., 2007). In previous studies, a stereological correction was commonly applied to convert the mean line-intercept length from a 2-D section to the mean grain diameter in 3-D (Hansen et al., 2011; Hansen & Warren, 2015; Underwood, 1970, pages 80–93; Valcke et al., 2006). As the choice of 3D correction adds an additional layer of uncertainty to the data processing, we avoid any correction and simply use the mean line-intercept length, λ, as the microstructural length scale in our piezometric calibration.

2.3 Sensitivity Tests

As EBSD maps only examine a portion of a deformed material, we devised two tests to assess whether a mapped area is representative of the bulk deformation. These tests examine the effect of the size and spatial resolution of the map on the measured values of mean intercept length. MATLAB® scripts to perform these tests are presented in the Supplemental Material (Text S1).

As increasing the step size of an EBSD map leads to overestimates of grain size (Cross et al., 2017; Humphreys, 2001), we tested the influence of step size on measured subgrain size. We evaluated the spatial resolution by implementing the same step size analysis test as Cross et al. (2017). In this procedure, the resolution of the map is artificially reduced (i.e., the effective step size increased) by selecting subsets of points in the map on a regular grid. The line-intercept length is then measured and compared to the mean-line intercept length associated with the smallest step size, λ_{best}. We refer to the ratio of λ to λ_{best} as the intercept variation factor. The spatial resolution is deemed sufficient if the measured mean intercept length is not sensitive to the effective step size. For each sample in Figures 1d and S2, decreasing the pixels per intercept length (defined as the λ_{best} divided by the effective step size) had an insignificant effect on the mean line-intercept length. The presence of an asymptote at an intercept variation factor of 1 is evidence that step size is small enough to capture the mean intercept length.

In the second test, we evaluated the size of the map relative to the mean intercept length, that is, whether a sufficient number of intercepts were measured for their mean value to be representative of the sample mean. We propose that, rather than being fixed (Humphreys, 2001, 2004; Valcke et al., 2006), the number of required subgrains (or intercept lengths) is likely to depend on the variance of the true subgrain-size distribution. Therefore, for each map, we tested the effect of map area on the mean intercept length by measuring the mean intercept length from a centred sub-area of the original map. Initially, this sub-area was 1% of the size of the original map. We then measured the mean intercept

length as the sub-area was progressively increased in size. As the size of the sub-area increases, the mean intercept length should asymptotically approach the mean for the entire map, indicating the full map area is sufficiently large. Examples of the area-analysis technique are presented in Figures 1e and S3. Samples that demonstrated a strong dependence of mean line-intercept length on the size of the sub-area (e.g., Figure S4) were mapped multiple times. The mean intercept length was then calculated as the average intercept length across all the maps to ensure representative measurement.

3. Results

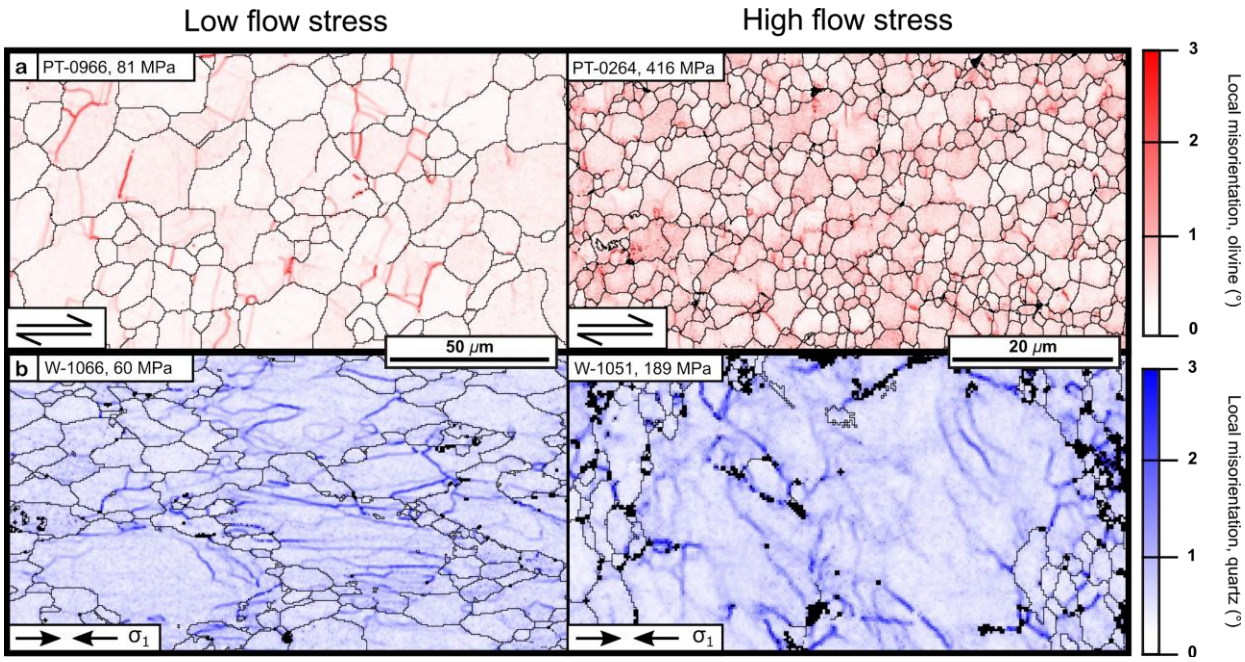

Figure 2: Maps of local misorientation for (a) olivine and (b) quartz samples deformed at low and high flow stresses. Black lines are grain boundaries (misorientation ≥ 10°). Unindexed pixels are also plotted in black. Experiments conducted at high flow stresses have higher densities of subgrain boundaries.

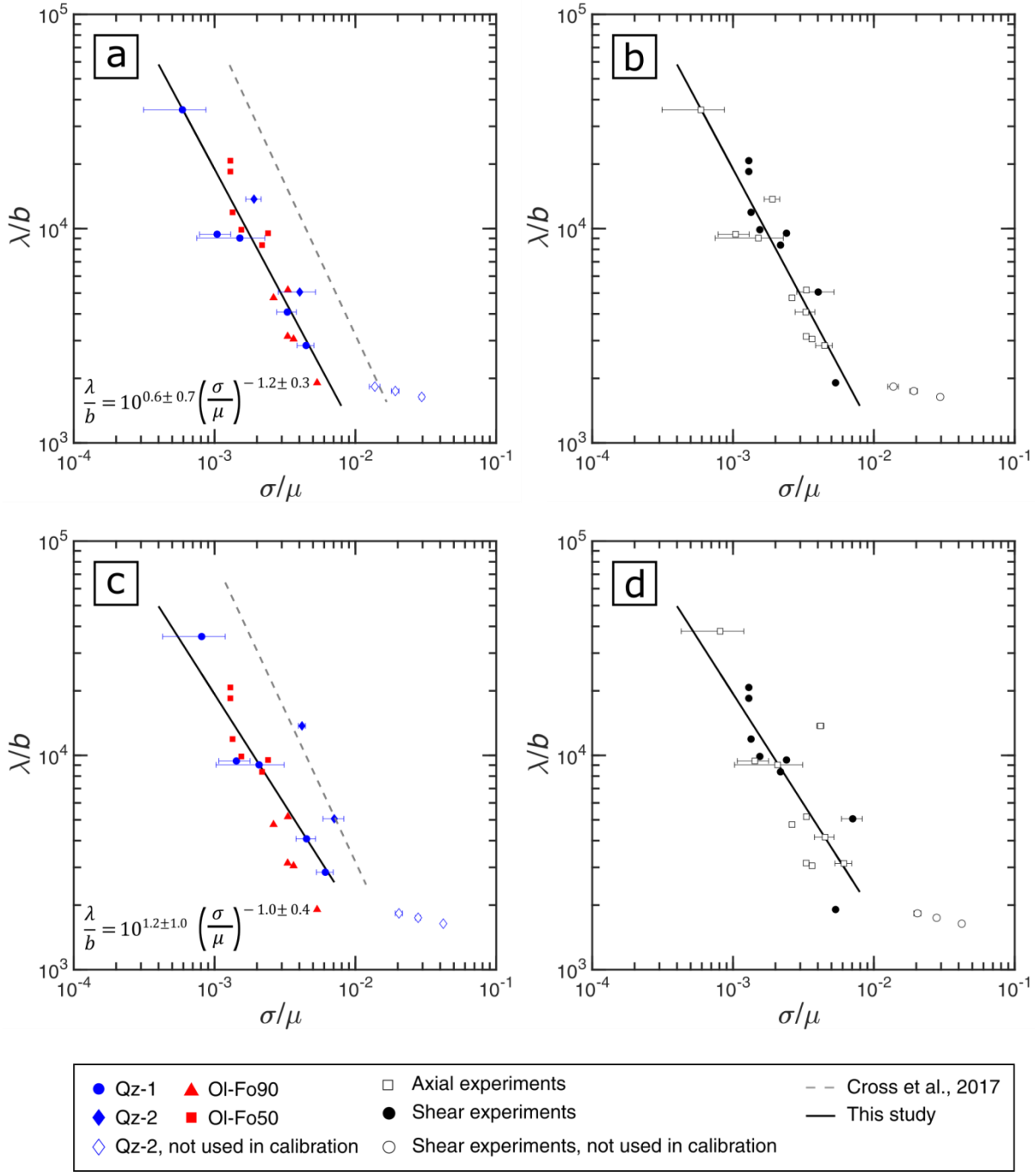

Figure 3: Mean line-intercept length, normalised by the Burgers vector as a function of the equivalent stress, normalised by the shear modulus. In (a) and (b) the correction from Holyoke and Kronenberg (2010) was applied to the quartz data, whereas in (c) and (d) the correction was not applied. (a) and (c) data are coloured by phase, with the recrystallised grain-size piezometer of Cross et al. (2017), also calibrated for EBSD, plotted for

comparison. (b) and (d) plot the same data as in (a) and (c), respectively, coloured by deformation geometry. Axial experiments refer to those conducted in pure shear and shear experiments refer to those conducted in general shear or simple shear.

To identify a general piezometric relationship applicable for both quartz and olivine, the equivalent stress and the mean intercept length were normalised by the shear modulus μ and the Burgers vector *b* respectively. We then explored the effect of the choice of critical misorientation angle on mean intercept length. We tested angles ranging from 1° to 10° (e.g., Figure 1c). We did not evaluate critical misorientation angles below 1°, the minimum angle that can be measured repeatedly and accurately with Hough-based EBSD (Humphreys, 2001, 2004; Wallis et al., 2016). Also we did not evaluate critical misorientation angles above 10° as we consider misorientations of >10° to be grain boundaries rather than subgrain boundaries. For all values of the critical misorientation angle, in all three datasets, the mean intercept length exhibits a power-law relationship with the equivalent stress (Figure S5). The three datasets coincide best at lower critical misorientation angles. The discrepancy between the quartz datasets and the olivine dataset increases as a function of increasing critical misorientation angle. Therefore, we used a critical misorientation angle of 1° in our calibrations.

We fit a power-law equation using least squares linear regression on the logarithmic transformation of mean intercept length against equivalent stress, yielding the following equations:

$$\frac{\lambda}{b} = 10^{0.6\pm0.7}\left(\frac{\sigma}{\mu}\right)^{-1.2\pm0.3} \quad \text{(eq.1)}$$

and

$$\frac{\lambda}{b} = 10^{1.2\pm1.0}\left(\frac{\sigma}{\mu}\right)^{-1.0\pm0.4} \quad \text{(eq.2).}$$

Equations 1 and 2 represent piezometers with and without the calibration of Holyoke and Kronenberg (2010) discussed above in Section 2.11, respectively. Uncertainties are reported as 95% confidence

intervals. Here we use b = 5.10x10^{-4} μm or 5×10^{-4} μm and μ = 4.2×10^{4} MPa or 7.78/6.26×10^{4} MPa for quartz and olivine (Fo_{90}/Fo_{50}), respectively (see supplementary Text S2 for discussion).

4. Discussion

The organization of dislocations into subgrain boundaries is driven by the associated reduction in the strain energy of the system (e.g., Raj & Pharr, 1986; Read, 1953, page 226). During deformation, the mean subgrain size varies systematically with the applied stress. Normalising the stress by the shear modulus and the subgrain size by the Burgers vector collapses mineral-specific piezometers into a single relationship (e.g., Twiss, 1986). Our results thus define a subgrain-size piezometer, which can be used on multiple minerals. As our piezometer is calibrated by EBSD, it differs from calibrations obtained by different measurement techniques (Durham & Goetze, 1977; Goetze, 1975; Karato et al., 1980; Mercier et al., 1977; Toriumi, 1979). We also provide a set of tests that assess the suitability of a dataset for analysis by this method based on factors including the number of linear intercepts, the step size, and the map area. The ability to perform these tests routinely in an automated and objective manner provides clear benefits over existing quality control measures (e.g., Humphreys, 2001, 2004; Valcke et al., 2006).

Subgrain-size piezometry is beneficial compared to grain-size piezometry in several ways. First, the most significant advantage of subgrain-size piezometry over grain-size piezometry is that the former is insensitive to the presence of secondary minerals and the pinning of grain boundaries (Hansen & Warren, 2015; White, 1979). As most rocks are polymineralic and the presence of secondary phases leads to smaller-than-expected recrystallised grains, the majority of existing stress estimates were derived from spatially restricted monomineralic rocks or domains. In contrast, in polymineralic rocks, subgrain-size piezometry should record the average stress supported by the analysed phase, regardless of the fraction of secondary phases. Thus, the subgrain-size piezometer can be used to analyse the stress supported by each phase deforming by dislocation creep in polymineralic rocks. Consequently, grain-

size piezometry based estimates of stresses supported by the lithosphere (e.g., Behr & Platt, 2011; Weathers et al., 1979; White, 1979) can be tested against new data acquired using subgrain-size piezometry on more representative rock types.

Grain-size piezometry also requires the user to distinguish between recrystallised and relict grains, the proportions of which depend on total strain. Previously, the bimodal grain-size distribution of partially recrystallised rocks allowed the characterization of recrystallised and relict grains on the basis of size (e.g., Post & Tullis, 1999; Stipp & Tullis, 2003). This method truncates the grain-size distribution, thereby modifying the mean grain size and the resulting stress calculated from that grain size. More recent work used the degree of intracrystalline lattice distortion within each grain to identify recrystallised grains on the assumption that relict grains have a greater degree of internal distortion than recrystallised grains (Cross et al., 2017). Although this new method provides a working calibration, it adds additional steps and assumptions to the analysis. In deforming materials with active subgrain formation, both recrystallized and relict grains develop subgrain boundaries which fall on a single piezometric relationship (Ross et al., 1980). As our calibration contains subgrains both from relict and recrystallised grains, as long as both sets of grains contain subgrains in the sample to be analysed, no distinction between them is necessary in measuring subgrain size. Instead, we only need to define a critical misorientation angle. The 1° critical misorientation angle fits with previous observations that subgrain boundaries tend to have misorientation angles < 2° at strains of 15% and < 5° at strains of 50% (Pennock et al., 2005) In addition, Trimby et al. (1998), observed subgrains in relict and recrystallized grains were the same size based on a 1° critical misorientation.

Finally, subgrain-size piezometry is independent of flow geometry. In contrast, samples deformed in general shear and axial compression may exhibit different grain sizes at the same equivalent stress (Heilbronner & Kilian, 2017). As observed by Heilbronner and Kilian (2017), different kinematics in subdomains of deformed quartzites lead to different crystallographic preferred orientations (CPOs). Different CPOs may reflect differences in the activity of different slip systems, which in turn may affect

298 the mean size of recrystallized grains. Thus, as demonstrated in the compilation of data for quartz
299 presented by Tokle et al. (2019), experiments conducted in simple shear yield a different grain-size
300 piezometer than experiments conducted in axial compression. To explore whether this hypothesis holds
301 true for subgrain sizes, we regrouped the data according to whether the samples were deformed in a pure
302 shear (i.e., axial compression) or general or simple shear, geometry. In Figures 3b and 3d, there is no
303 obvious dependence of the mean intercept length on the deformation geometry. Therefore, we suggest
304 that our single subgrain-size piezometer can be applied to a wide range of rocks, regardless of flow
305 geometry or CPO.

306 It is necessary to highlight two potential limitations of subgrain-size piezometry. First, it appears
307 that the observed relationship between subgrain size and stress is not applicable to deformation at high
308 stresses (Figure 3). The relationship between subgrain size and stress may change at higher stresses as
309 the recrystallization mechanisms changes, similar to the relationships observed for the size of
310 recrystallised grains of quartz (Stipp & Tullis, 2003), which is why the three samples deformed in this
311 high-stress regime were not included in our calibrations. Similarly, differences in the processes of
312 subgrain formation or in the mechanisms of dynamic recrystallisation might require different calibrations
313 at significantly low stresses (e.g., Valcke et al., 2007, 2015; Stipp et al., 2010). Therefore, we
314 recommend that our piezometer should be applied over the normalised subgrain size and stress range
315 over which it was calibrated. This range corresponds to mean line-intercept lengths of 1–9 μm for
316 olivine and 1–18 μm for quartz and a similar range for other silicate minerals. These limits on subgrain
317 size correspond to stress ranges of 60–420 MPa and 20–240 MPa for olivine and quartz, respectively.

318 Second, the potential for modifying subgrain size through static annealing or stress relaxation
319 after deformation remains poorly constrained. Ross et al. (1980) suggested that subgrains record the
320 highest stress in rocks subjected to complex deformation histories. However, we demonstrate a strong
321 correlation between subgrain size and final stress is apparent, even in cases in which the larger stresses
322 were experienced earlier in the deformation history (Hansen et al., 2012; Holyoke & Tullis, 2006).

Furthermore, experiments in steel by Qin et al. (2003) revealed that subgrains were only able to coarsen with additional strain while under stress of a reduced magnitude, whereas they did not coarsen during static annealing. These observations suggest that subgrain sizes best reflect the last increments of deformation, although further work is clearly required to fully investigate the mobility of subgrain boundaries in minerals. If the subsequent modification of subgrain size occurs on a different timescale than the modification of other microstructural features such as dislocation density or recrystallized grain size, then combined analysis using multiple piezometers may yield information about complex stress histories (Kohlstedt & Weathers, 1980; White, 1979).

5. Conclusions

1. We present a subgrain-size piezometer calibrated for EBSD with a 1° critical misorientation angle. This piezometer, which was derived from data for olivine and quartz should be applicable to other phases.
2. The size of subgrains calculated based on a critical misorientation angle of 1° appears to be independent of the deformation geometry, that is, whether the specimen is deformed in simple/general shear or pure shear.
3. It is recommended that our piezometer should be applied over the normalised subgrain size and stress range with which it was calibrated. This corresponds to mean line-intercept lengths of 1 to 9 μm for olivine and 1 to 18 μm for quartz corresponding to stresses of 60 – 420 MPa and 20 – 240 MPa, respectively
4. MATLAB® scripts, provided in the Supplemental Material, can be used to test the suitability of input data for stress estimates specifically in terms of spatial resolution and size of the data set.

Acknowledgements

The authors thank Andrew Cross for useful discussions. Jon Wade and Phillip Gopon are gratefully acknowledged for technical support on the SEM. This research was supported by the NERC Environmental Research DTP, University of Oxford, RMG, and National Science Foundation (NSF) Awards EAR-1755805 to DLK, EAR-1806791 to KMK and EAR-1848380 to CWH. In addition, Qz-2 experiments were performed by CWH with support from NSF grants EAR-0208150 to Jan Tullis and EAR-1321882 to CWH and Andreas K. Kronenberg. EBSD data sets are currently available from Oxford University Research Archive (DOI: https://doi.org/10.5287/bodleian:9R9GMgO25).

References

Abramson, E. H., Brown, J. M., Slutsky, L. J., & Zaug, J. (1997). The elastic constants of San Carlos olivine to 17 GPa. *Journal of Geophysical Research*, *102*(B6), 12253–12263. https://doi.org/10.1029/97JB00682

Austin, N., Evans, B., Herwegh, M., & Ebert, A. (2008). Strain localization in the Morcles nappe (Helvetic Alps, Switzerland). *Swiss Journal of Geosciences*, *101*(2), 341–360. https://doi.org/10.1007/s00015-008-1264-2

Behr, W. M., & Platt, J. P. (2011). A naturally constrained stress profile through the middle crust in an extensional terrane. *Earth and Planetary Science Letters*, *303*(3), 181–192. https://doi.org/10.1016/j.epsl.2010.11.044

Behr, W. M., & Platt, J. P. (2014). Brittle faults are weak, yet the ductile middle crust is strong: Implications for lithospheric mechanics. *Geophysical Research Letters*, *41*(22), 8067–8075. https://doi.org/10.1002/2014GL061349

Biberger, M., & Blum, W. (1992). Subgrain boundary migration during creep of lif: I. Recombination of subgrain boundaries. *Philosophical Magazine A*, *65*(3), 757–770. https://doi.org/10.1080/01418619208201548

Birch, F. (1966). Compressibility; elastic constants. In S.P. Clark (Eds.), *Handbook of Physical Constants* (pp. 169). New York, NY: The Geological Society of America.

Britton, T. B., & Wilkinson, A. J. (2011). Measurement of residual elastic strain and lattice rotations with high resolution electron backscatter diffraction. *Ultramicroscopy*, *111*(8), 1395–1404. https://doi.org/10.1016/j.ultramic.2011.05.007

Britton, T. B., & Wilkinson, A. J. (2012). Stress fields and geometrically necessary dislocation density distributions near the head of a blocked slip band. *Acta Materialia*, *60*(16), 5773–5782. https://doi.org/10.1016/j.actamat.2012.07.004

Cross, A. J., Prior, D. J., Stipp, M., & Kidder, S. (2017). The recrystallized grain size piezometer for quartz: An EBSD-based calibration. *Geophysical Research Letters*, *44*(13), 6667–6674. https://doi.org/10.1002/2017GL073836

Deer, W. A., Howie, R. A., & Zussman, J. (1992). *An introduction to the rock-forming minerals.* 2nd ed. Harlow, Essex, England: New York, NY: Longman Scientific & Technical.

Durham, W. B., & Goetze, C. (1977). Plastic flow of oriented single crystals of olivine: 1. Mechanical data. *Journal of Geophysical Research*, *82*(36), 5737–5753. https://doi.org/10.1029/JB082i036p05737

Evans, B., Renner, J., & Hirth, G. (2001). A few remarks on the kinetics of static grain growth in rocks. *International Journal of Earth Sciences*, *90*(1), 88–103. https://doi.org/10.1007/s005310000150

Friedman, M., & Higgs, N. G. (1981). Calcite Fabrics in Experimental Shear Zones. In N.L. Carter, M. Friedman, J.M. Logan, D.W. Stearns (Eds.), *Mechanical Behavior of Crustal Rocks: The Handin Volume* (pp. 11–27). Washington, DC: American Geophysical Union.

Gleason, G. C., & Tullis, J. (1995). A flow law for dislocation creep of quartz aggregates determined with the molten salt cell. *Tectonophysics*, *247*(1-4), 1–23. https://doi.org/10.1016/0040-1951(95)00011-B

Goetze, C. (1975). Sheared Iherzolites: From the point of view of rock mechanics. *Geology*, *3*(4), 172–

173. https://doi.org/10.1130/0091-7613(1975)3<172:SIFTPO>2.0.CO;2

Gueydan, F., Mehl, C., & Parra, T. (2005). Stress-strain rate history of a midcrustal shear zone and the onset of brittle deformation inferred from quartz recrystallized grain size. In D. Gapais, J.P. Brun & P.R. Cobbold (Eds.), *Deformation Mechanisms, Rheology and Tectonics: from Minerals to the lithosphere* (Special Publications 243, p. 127–142) London, UK: *Geological Society*. https://doi.org/10.1029/GM024p0011

Haertel, M., & Herwegh, M. (2014). Microfabric memory of vein quartz for strain localization in detachment faults: A case study on the Simplon fault zone. *Journal of Structural Geology*, 68, 16–32. https://doi.org/10.1016/j.jsg.2014.08.001

Hansen, L. N., & Warren, J. M. (2015). Quantifying the effect of pyroxene on deformation of peridotite in a natural shear zone. *Journal of Geophysical Research, Solid Earth*, *120*(4), 2717–2738. https://doi.org/10.1002/2014JB011584

Hansen, L. N., Zimmerman, M. E., & Kohlstedt, D. L. (2011). Grain boundary sliding in San Carlos olivine: Flow law parameters and crystallographic-preferred orientation. *Journal of Geophysical Research, Solid Earth*, *116*(B8), B08201. https://doi.org/10.1029/2011JB008220

Hansen, L. N., Zimmerman, M. E., & Kohlstedt, D. L. (2012). The influence of microstructure on deformation of olivine in the grain-boundary sliding regime. *Journal of Geophysical Research, Solid Earth*, *117*(B9), B09201. https://doi.org/10.1029/2012JB009305

Hansen, L. N., Cheadle, M. J., John, B. E., Swapp, S. M., Dick, H. J. B., Tucholke, B. E., & Tivey, M. A. (2013). Mylonitic deformation at the Kane oceanic core complex: Implications for the rheological behavior of oceanic detachment faults. *Geochemistry, Geophysics, Geosystems*, *14*(8), 3085–3108. https://doi.org/10.1002/ggge.20184

Heilbronner, R., & Kilian, R. (2017). The grain size(s) of Black Hills Quartzite deformed in the dislocation creep regime. *Solid Earth*, *8*(6), 1071–1093. https://doi.org/10.5194/se-8-1071-2017

Heilbronner, R., & Tullis, J. (2002). The effect of static annealing on microstructures and

crystallographic preferred orientations of quartzites experimentally deformed in axial compression and shear. *Geological Society, London, Special Publications*, *200*(1), 191–218. https://doi.org/10.1144/GSL.SP.2001.200.01.12

Heilbronner, R., & Tullis, J. (2006). Evolution of c axis pole figures and grain size during dynamic recrystallization: Results from experimentally sheared quartzite. *Journal of Geophysical Research*, *111*(B10), B10202. https://doi.org/10.1029/2005JB004194

Hiraga, T., Tachibana, C., Ohashi, N., & Sano, S. (2010). Grain growth systematics for forsterite ± enstatite aggregates: Effect of lithology on grain size in the upper mantle. *Earth and Planetary Science Letters*, *291*(1-4), 10–20. https://doi.org/10.1016/j.epsl.2009.12.026

Hirth, G., & Tullis, J. (1992). Dislocation creep regimes in quartz aggregates. *Journal of Structural Geology*, *14*(2), 145–159. https://doi.org/10.1016/0191-8141(92)90053-Y

Hirth, G., Teyssier, C., & Dunlap, J. W. (2001). An evaluation of quartzite flow laws based on comparisons between experimentally and naturally deformed rocks. *International Journal of Earth Sciences*, *90*, 77–87. https://doi.org/10.1007/s005310000152

Holyoke, C. W., III, & Kronenberg, A. K. (2010). Accurate differential stress measurement using the molten salt cell and solid salt assemblies in the Griggs apparatus with applications to strength, piezometers and rheology. *Tectonophysics*, *494*(1-2), 17–31. https://doi.org/10.1016/j.tecto.2010.08.001

Holyoke, C. W., III, & Kronenberg, A. K. (2013). Reversible water weakening of quartz. *Earth and Planetary Science Letters*, *374*, 185–190. https://doi.org/10.1016/j.epsl.2013.05.039

Holyoke, C. W., III, & Tullis, J. (2006). Mechanisms of weak phase interconnection and the effects of phase strength contrast on fabric development. *Journal of Structural Geology*, *28*(4), 621–640. https://doi.org/10.1016/j.jsg.2006.01.008

Humphreys, F. J. (2001). Grain and subgrain characterisation by electron backscatter diffraction. *Journal of Materials Science*, *36*(16), 3833–3854. https://doi.org/10.1023/A:1017973432592

Humphreys, F. J. (2004). Characterisation of fine-scale microstructures by electron backscatter diffraction (EBSD). *Scripta Materialia*, *51*(8), 771–776. https://doi.org/10.1016/j.scriptamat.2004.05.016

Jaroslow, G. E., Hirth, G., & Dick, H. J. B. (1996). Abyssal peridotite mylonites: implications for grain-size sensitive flow and strain localization in the oceanic lithosphere. *Tectonophysics*, *256*(1), 17–37. https://doi.org/10.1016/0040-1951(95)00163-8

Karato, S.-I. (2012). *Deformation of Earth Materials: An Introduction to the Rheology of Solid Earth* Cambridge UK: Cambridge University Press.

Karato, S.-I., Toriumi, M., & Fujii, T. (1980). Dynamic recrystallization of olivine single crystals during high temperature creep. *Geophysical Research Letters*, *7*(9), 649–652. https://doi.org/10.1029/GL007i009p00649

Kohlstedt, D. L., & Weathers, M. S. (1980). Deformation-Induced Microstructures, Paleopiezometers, and Differential Stresses in Deeply Eroded Fault Zones. *Journal of Geophysical Research*, *85*(B11), 6269–6285. https://doi.org/10.1029/JB085iB11p06269

Linckens, J., Herwegh, M., Müntener, O., & Mercolli, I. (2011). Evolution of a polymineralic mantle shear zone and the role of second phases in the localization of deformation. *Journal of Geophysical Research*, *116*(B6), B06210. https://doi.org/10.1029/2010JB008119

Luton, M. J., & Sellars, C. M. (1969). Dynamic recrystallization in nickel and nickel-iron alloys during high temperature deformation. *Acta Metallurgica*, *17*(8), 1033–1043. https://doi.org/10.1016/0001-6160(69)90049-2

Mackwell, S. J., & Paterson, M. S. (2002). New Developments in Deformation Studies: High-Strain Deformation. *Reviews in Mineralogy and Geochemistry*, *51*(1), 1–19. https://doi.org/10.2138/gsrmg.51.1.1

Mao, Z., Fan, D., Lin, J.-F., Yang, J., Tkachev, S.N., Zhuravlev, K., & Prakapenka, V.B. (2015). Elasticiy of single-crystal olivine at high pressures and temperatures. *Earth and Planetary Science*

Letters, *426*, 204–215. https://doi.org/10.1016/j.epsl.2015.06.045.

Mercier, J.-C. C., Anderson, D. A., & Carter, N. L. (1977). Stress in the Lithosphere: Inferences from Steady State Flow of Rocks. In M.Wyss (Eds.), *Stress in the Earth* (pp. 199–226). Birkhäuser, Basel. https://doi.org/10.1007/978-3-0348-5745-1_12

Mingard, K. P., Roebuck, B., Bennett, E. G., Thomas, M., Wynne, B. P., & Palmiere, E. J. (2007). Grain size measurement by EBSD in complex hot deformed metal alloy microstructures. *Journal of Microscopy*, *227*(3), 298–308. https://doi.org/10.1111/j.1365-2818.2007.01814.x

Paterson, M. S. (1990), Rock deformation experimentation, In A. G. Duba and W. B . Durham, H. C. Heardm J.w. Handin, H.F.Wang (Eds.), *The Brittle Ductile Transition in Rocks, The Heard Volume, Geophysical Monograph Series* (Vol. 56, pp. 187–194). AGU, Washington, D. C: American Geophysical Union.

Paterson, M. S., & Olgaard, D. L. (2000). Rock deformation tests to large shear strains in torsion. *Journal of Structural Geology*, *22*(9), 1341–1358. https://doi.org/10.1016/S0191-8141(00)00042-0

Peng, Z., & Redfern, S. A. T. (2013). Mechanical properties of quartz at the α-β phase transition: Implications for tectonic and seismic anomalies. *Geochemistry, Geophysics, Geosystems*, *14*(1), 18–28. https://doi.org/10.1029/2012GC004482

Pennock, G. M., Drury, M. R., & Spiers, C. J. (2005). The development of subgrain misorientations with strain in dry synthetic NaCl measured using EBSD. *Journal of Structural Geology*, *27*(12), 2159–2170. https://doi.org/10.1016/j.jsg.2005.06.013

Platt, J. P., & De Bresser, J. H. P. (2017). Stress dependence of microstructures in experimentally deformed calcite. *Journal of Structural Geology*, *105*, 80–87. https://doi.org/10.1016/j.jsg.2017.10.012

Poirier, J. P., & Nicolas, A. (1975). Deformation-Induced Recrystallization Due to Progressive Misorientation of Subgrains, with Special Reference to Mantle Peridotites. *The Journal of Geology*, *83*(6), 707–720. https://doi.org/10.1086/628163

Pommier, A., Leinenweber, K., Kohlstedt, D. L., Qi, C., Garnero, E. J., Mackwell, S. J., & Tyburczy, J. A. (2015). Experimental constraints on the electrical anisotropy of the lithosphere–asthenosphere system. *Nature*, *522*, 202. https://doi.org/10.1038/nature14502

Post, A., & Tullis, J. (1999). A recrystallized grain size piezometer for experimentally deformed feldspar aggregates. *Tectonophysics*, *303*(1), 159–173. https://doi.org/10.1016/S0040-1951(98)00260-1

Qin, Y., Götz, G., & Blum, W. (2003). Subgrain structure during annealing and creep of the cast martensitic Cr-steel G-X12CrMoWVNbN 10-1-1. *Materials Science and Engineering: A, 341*(1), 211–215. https://doi.org/10.1016/S0921-5093(02)00215-0

Raj, S. V., & Pharr, G. M. (1986). A Compilation and Analysis of Data for the Stress Dependence of the Subgrain size. *Materials Science and Engineering*, *81*, 217–237. https://doi.org/10.1016/0025-5416(86)90265-X

Read, W. T. (1953). *Dislocations in crystals*. New York, NY: McGraw-Hill.

Ross, J. V., Ave Lallemant, H. G., & Carter, N. L. (1980). Stress dependence of recrystallized-grain and subgrain size in olivine. *Tectonophysics*, *70*(1-2), 39–61. https://doi.org/10.1016/0040-1951(80)90020-7

Rutter, E. H. (1995). Experimental study of the influence of stress, temperature, and strain on the dynamic recrystallization of Carrara marble. *Journal of Geophysical Research, Solid Earth*, 100(B12), 24651–24663. https://doi.org/10.1029/95JB02500

Schmid, S. M., Paterson, M. S., & Boland, J. N. (1980). High temperature flow and dynamic recrystallization in carrara marble. *Tectonophysics*, *65*(3), 245–280. https://doi.org/10.1016/0040-1951(80)90077-3

Shimizu, I. (1998). Stress and temperature dependence of recrystallized grain size: A subgrain misorientation model. *Geophysical Research Letters*, *25*(22), 4237–4240. https://doi.org/10.1029/1998GL900136

Shimizu, I. (2008). Theories and applicability of grain size piezometers: The role of dynamic

recrystallization mechanisms. *Journal of Structural Geology*, *30*(7), 899–917. https://doi.org/10.1016/j.jsg.2008.03.004

Skemer, P., Warren, J. M., Kelemen, P. B., & Hirth, G. (2010). Microstructural and Rheological Evolution of a Mantle Shear Zone. *Journal of Petrology*, *51*(1-2), 43–53. https://doi.org/10.1093/petrology/egp057

Skemer, P., Warren, J. M., Hansen, L. N., Hirth, G., & Kelemen, P. B. (2013). The influence of water and LPO on the initiation and evolution of mantle shear zones. *Earth and Planetary Science Letters*, *375*, 222–233. https://doi.org/10.1016/j.epsl.2013.05.034

Smith, C. S. (1948). Zener pinning. *Transactions of the Metallurgical Society of AIME*, *175*, 15–51. New York, NY: American institute of mining metallurgical and petroleum engineers.

Speckbacher, R., Behrmann, J. H., Nagel, T. J., Stipp, M., & Devey, C. W. (2011). Splitting a continent: Insights from submarine high-resolution mapping of the Moresby Seamount detachment, offshore Papua New Guinea. *Geology*, *39*(7), 651–654. https://doi.org/10.1130/G31931.1

Stipp, M., & Tullis, J. (2003). The recrystallized grain size piezometer for quartz. *Geophysical Research Letters*, *30*(21), 2088. https://doi.org/10.1029/2003GL018444

Stipp, M., Stünitz, H., Heilbronner, R., & Schmid, M. (2002). Dynamic recrystallization of quartz: correlation between natural and experimental conditions. In: S. De Meer, M.R. Drury, J.H.P. De Bresser & G.M. Pennock, (Eds.): *Deformation Mechanisms, Rheology and Tectonics: Current Status and Future Perspectives* (Special Publications 200, pp. 171-190). London, UK: Geological Society of London,. https://doi.org/10.1144/GSL.SP.2001.200.01.11

Stipp, M., Tullis, J., Scherwath, M., & Behrmann, J. H. (2010). A new perspective on paleopiezometry: Dynamically recrystallized grain size distributions indicate mechanism changes. *Geology*, 38(8), 759–762. https://doi.org/10.1130/G31162.1

Tasaka, M., Zimmerman, M. E., & Kohlstedt, D. L. (2016). Evolution of the rheological and microstructural properties of olivine aggregates during dislocation creep under hydrous conditions.

Journal of Geophysical Research, Solid Earth, 121(1), 92–113. https://doi.org/10.1002/2015JB012134

Tasaka, M., Zimmerman, M. E., & Kohlstedt, D. L. (2017). Rheological weakening of Olivine + Orthopyroxene aggregates due to phase mixing: 1. Mechanical Behavior. *Journal of Geophysical Research, Solid Earth*, *122*(10), 7584–7596. https://doi.org/10.1002/2017JB014333

Tasaka, M., Zimmerman, M. E., Kohlstedt, D. L., Stünitz, H., & Heilbronner, R. (2017). Rheological weakening of olivine+ orthopyroxene aggregates due to phase mixing: Part 2. Microstructural development. *Journal of Geophyical Research, Solid Earth*, *122*(10), 7597–7612. https://doi.org/10.1002/2017JB014311

Thatcher, W., & Pollitz, F. F. (2008). Temporal evolution of continental lithospheric strength in actively deforming regions. *GSA Today: A Publication of the Geological Society of America*, *18*(4/5), 4–11. https://doi.org/10.1130/GSAT01804-5A

Tokle, L., Hirth, G., & Behr, W. M. (2019). Flow laws and fabric transitions in wet quartzite. *Earth and Planetary Science Letters, 505*, 152–161. https://doi.org/10.1016/j.epsl.2018.10.017

Toriumi, M. (1979). Relation between dislocation density and subgrain size of naturally deformed olivine in peridotites. *Contributions to Mineralogy and Petrology*, *68*(2), 181–186. https://doi.org/10.1007/BF00371899

Trimby, P., Day, A., Mehnert, K., & Schmidt, N.-H. (2002). Is fast mapping good mapping? A review of the benefits of high-speed orientation mapping using electron backscatter diffraction. *Journal of Microscopy*, *205*(3), 259–269. https://doi.org/10.1046/j.1365-2818.2002.00995.x

Trimby, P. W., Prior, D. J., & Wheeler, J. (1998). Grain boundary hierarchy development in a quartz mylonite. *Journal of Structural Geology*, 20(7), 917–935. https://doi.org/10.1016/S0191-8141(98)00026-1

Twiss, R. J. (1986). Variable sensitivity piezometric equations for dislocation density and subgrain diameter and their relevance to olivine and quartz. In B. E. Hobbs & H. C. Heard (Eds.), *Mineral*

570 *and Rock deformation: Laboratory studies:The Paterson Volume*. Washington, D.C: American
571 Geophysical Union. https://doi.org/10.1029/GM036p0247
572 Underwood, E. E. (1970). *Quantitative stereology*. Addison-Wesley Publishing Company.
573 Valcke, S. L. A., & De Bresser, J. H. P. (2015). Influence of deformation conditions on the development
574 of heterogeneous recrystallization microstructures in experimentally deformed Carrara marble.
575 *Geological Society*. http://dx.doi.org/10.1144/SP409.4
576 Valcke, S. L. A., Drury, M. R., de Bresser, J. H. P., & Pennock, G. M. (2007). Quantifying
577 Heterogeneous Microstructures: Core and Mantle Subgrains in Deformed Calcite. *Materials*
578 *Science Forum*. https://doi.org/10.4028/0-87849-434-0.307
579 Valcke, S. L. A., Pennock, G. M., Drury, M. R., & De Bresser, J. H. P. (2006). Electron backscattered
580 diffraction as a tool to quantify subgrains in deformed calcite. *Journal of Microscopy*, *224*(3), 264–
581 276. https://doi.org/10.1111/j.1365-2818.2006.01698.x
582 Van der Wal, D., Chopra, P., Drury, M., & Gerald, J. F. (1993). Relationships between dynamically
583 recrystallized grain size and deformation conditions in experimentally deformed olivine rocks.
584 *Geophysical Research Letters*, *20*(14), 1479–1482. https://doi.org/10.1029/93GL01382
585 Wallis, D., Hansen, L. N., Britton, T. B., & Wilkinson, A. J. (2016). Geometrically necessary dislocation
586 densities in olivine obtained using high-angular resolution electron backscatter diffraction.
587 *Ultramicroscopy*, *168*, 34–45. https://doi.org/10.1016/j.ultramic.2016.06.002
588 Wallis, D., Parsons, A. J., & Hansen, L. N. (2017). Quantifying geometrically necessary dislocations in
589 quartz using HR-EBSD: Application to chessboard subgrain boundaries. *Journal of Structural*
590 *Geology*. https://doi.org/10.1016/j.jsg.2017.12.012
591 Warren, J. M., & Hirth, G. (2006). Grain size sensitive deformation mechanisms in naturally deformed
592 peridotites. *Earth and Planetary Science Letters*, *248*(1–2), 438–450.
593 https://doi.org/10.1016/j.epsl.2006.06.006
594 Weathers, M. S., Bird, J. M., Cooper, R. F., & Kohlstedt, D. L. (1979). Differential stress determined

595 from deformation-induced microstructures of the Moine Thrust Zone. *Journal of Geophysical*
596 *Research, Solid Earth*, *84*(B13), 7495–7509. https://doi.org/10.1029/JB084iB13p07495
597 Wex, S., Mancktelow, N. S., Camacho, A., & Pennacchioni, G. (2019). Interplay between seismic
598 fracture and aseismic creep in the Woodroffe Thrust, central Australia—Inferences for the rheology
599 of relatively dry continental mid-crustal levels. *Tectonophysics*, *758*, 55–72.
600 https://doi.org/10.1016/j.tecto.2018.10.024
601 White, S. (1979). Grain and sub-grain size variations across a mylonite zone. *Contributions to*
602 *Mineralogy and Petrology* , *70*(2), 193–202. https://doi.org/10.1007/BF00374448
603 Wilkinson, A. J. (1996). Measurement of elastic strains and small lattice rotations using electron back
604 scatter diffraction. *Ultramicroscopy*, *62*(4), 237–247. https://doi.org/10.1016/0304-3991(95)00152-
605 2
606 Wilkinson, A. J., & Randman, D. (2010). Determination of elastic strain fields and geometrically
607 necessary dislocation distributions near nanoindents using electron back scatter diffraction.
608 *Philosophical Magazine*, *90*(9), 1159–1177. https://doi.org/10.1080/14786430903304145
609 Wilkinson, A. J., Meaden, G., & Dingley, D. J. (2006). High resolution mapping of strains and rotations
610 using electron backscatter diffraction. *Materials Science and Technology*, *22*(11), 1271–1278.
611 https://doi.org/10.1179/174328406X130966

612